Illumination control in lensless imaging for EUV mask inspection and review

Iacopo Mochi, Hyun-Su Kim, Uldis Locans, Atoosa Dejkameh, Ricarda Nebling, Dimitrios Kazazis, and Yasin Ekinci

Paul Scherrer Institut, Villigen, Switzerland

ABSTRACT

Coherence control and flexible pupil fill play a key role in the imaging of EUV reticles. This is also true for lensless metrology applications based on coherent diffraction imaging. We describe the concept and the key components of a Fourier synthesis illuminator designed to provide the RESCAN microscope with flexible illumination capabilities and to improve its resolution limit. In particular, we discuss the characteristics of the three mirrors of the new illuminator and the requirements for their multilayer coating.

Keywords: EUV mask review, inspection, defects, lensless imaging, coherent diffraction imaging, ptychography.

1. INTRODUCTION

As technological progress in the infrastructure for EUV lithography moves towards future technology nodes, the feature sizes present on photomask and wafers keep shrinking and the requirements for EUV metrology become more demanding. Even if commercial solutions for actinic pattern mask inspection (APMI) and EUV mask review are available,[1,2] their cost of ownership remains relatively high and more development will likely be needed for future technology nodes.

In this scenario, we started exploring the possibility to carry out mask metrology with a lensless imaging approach based on coherent diffraction imaging (CDI). We developed the RESCAN microscope, a CDI-based EUV mask inspection platform operating at the Swiss Light Source synchrotron. In RESCAN, a sample is scanned with an EUV beam probe and a pixel detector collects the relative diffraction patterns. We then use ptychography to reconstruct the complex amplitude of the inspected sample and we compare it with an image of a reference area of the mask (die-to-die approach) or with an image calculated from the mask design (die-to-database approach) to identify the presence of defects.

We demonstrated lensless APMI with a defect sensitivity down to 50 nm. We also demonstrated that RESCAN can be used on pellicle-protected masks and allows to detect defects on the pellicle surface as well.[3]

The current illumination system of RESCAN has a fixed chief ray angle of 6º and a numerical aperture that can vary between 0.002 and 0.016. This setting causes a fundamental limitation on the performance of the microscope. In a lensless system, the resolution limit depends on the acceptance angle of the detector while in a traditional imaging device, it is linked to the numerical aperture of the objective optics. To increase the resolution in RESCAN, it should be sufficient to increase the acceptance angle of the detector by choosing a larger detector or by reducing its distance from the sample. Unfortunately, the multilayer on the surface of the EUV mask is designed to reflect light at a wavelength of 13.5 nm with an incidence angle between $-12º$ and $12º$ and, beyond this angle range, the mask reflectivity drops rapidly. This limits the theoretical resolution of RESCAN to about 48 nm.[4] To overcome this problem, we decided to upgrade our system with a Fourier synthesis illuminator[5,6] to shift the portions of the diffraction spectrum that are normally unreachable, in the high-reflectivity angular range of the EUV mask. This approach will enable us to increase the resolution of RESCAN and will give it the flexibility to operate with arbitrary pupil shapes, paving the way towards EUV lensless mask review.

In this paper we review the characteristics of the Fourier synthesis illuminator we designed and we discuss the main challenges in the realization of its optical components.

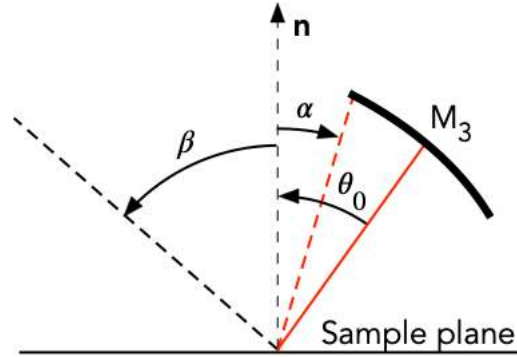Further author information: E-mail: iacopo.mochi@psi.ch

Figure 1. Diagram showing the chief ray angle θ_0, the maximum angle allowed by the multilayer β, and the minimum angle of incidence allowed by the condenser mirror α.

The parameters considered in the design of the illumination system are the single beam illumination NA, the probe size, shape, and intensity, the single-acquisition imaging NA, the maximum synthesizable imaging NA and the partial coherence of the single probe. To find a compromise between the optimal values of these parameters, we designed the three-mirror system shown in figure 2.

1.1 Probe size

In the current configuration of RESCAN, the sample is close to the focal point of the condenser optics and our probe takes the shape of an Airy pattern. This approach maximizes the photon density over a circular area with a radius of 2 to 3 μm, depending on the condenser defocus and on the size of the aperture stop we use, giving high intensity high-order diffraction structures, but causing saturation and blooming in the low-order diffraction peaks on detectors with a limited dynamic range. This can be addressed by stitching multiple exposure together to create a high dynamic range image of the diffraction pattern, but it is a time consuming and error-prone procedure. For this reason, we decided to spread out the energy over a larger area by re-imaging an out-of-focus plane of the illumination beam onto the sample surface. The maximum size D for the probe is limited by the coherence of the beam:[7]

$$\frac{\lambda}{\Delta\lambda} > \frac{D}{\delta}, \tag{1}$$

where δ is the smallest feature that can be reconstructed, λ is the wavelength and $\Delta\lambda$ is the illumination bandwidth. RESCAN illumination is provided by the XIL-II beamline which is equipped with a monochromator with $\lambda/\Delta\lambda = 1500$ at 13.5 nm. For a maximum achievable resolution limit of 20 nm, the largest probe size would be 30 μm.

1.2 Imaging NA

The new system is designed to enable complex illumination patterns and provide coherence control for advanced imaging. This will come at the expense of a longer acquisition time because, to generate an arbitrary illumination pattern, it will be necessary to collect various datasets corresponding to the elements of the pupil that we want to synthesize. At the same time, it is important to preserve the ability of the microscope to perform fast, high-coherence illumination imaging with a single illumination probe. The imaging numerical aperture along the axis parallel to the incidence plane (NA_Y) is limited by the extent of the condenser optics as shown in figure 1.[4] If α is the minimum incidence angle allowed by the condenser and β is the maximum reflection angle allowed by the multilayer on the EUV mask sample, the maximum non vignetted NA_Y value for a chief ray angle θ_0 is given by:

$$NA_Y = \min\left[\sin\left(\theta_0 + \alpha\right),\ \sin\left(\beta - \theta_0\right)\right], \tag{2}$$

and the maximum synthetic NA achievable is:

$$NA_{Y\max} = \sin\left(\beta - \alpha\right). \tag{3}$$

Assuming $\beta = 14°$, the current RESCAN configuration with a chief ray angle of illumination θ_0 of 6°and $\alpha = \theta_0$, has an effective NA_Y of 0.14. In the new system $\alpha = 3.5°$and the maximum synthetic $NA_{Y\max}$ is 0.18.

1.3 Illumination NA

In the current RESCAN configuration, the illumination NA can be varied by selecting aperture stops with different diameters. With a circular stop with 1 mm diameter, the illumination NA is 0.004. In the new design, with the same aperture size, we will have an illumination NA of 0.009 which translates into a reduced flux density on the detector and relaxes its dynamic range requirements.[8]

Stop diameter [mm]	Current		New	
	Probe size [μm]	NA	Probe size [μm]	NA
0.5	7.9	0.0021	5	0.0043
1.0	3.9	0.0042	10	0.0087
1.5	2.6	0.0062	15	0.0130
2.0	2.0	0.0083	20	0.0174

Table 1. Probe size as a function of the aperture stop diameter for the current and for the new optical configuration of RESCAN. In the current configuration, the condenser focuses the beam on the sample and the probe takes the shape of an Airy pattern; the probe size in this case is the Airy diameter. In the new configuration, the probe is an image of a defocused plane of the illumination beam and it has a circular shape.

2. THE FOURIER SYNTHESIS ILLUMINATOR

The current condenser of RESCAN will be substituted with the Fourier synthesis illuminator shown in figure 2. The new system will allow to synthesize larger and structured illumination pupils to extend the resolution of the microscope and to investigate the three dimensional properties of the EUV mask.

The EUV beam from the XIL-II beamline will be focused by a paraboloidal mirror M_1 and will be reflected by a tip-tilt mirror M_2 towards the condenser M_3. The points P and Q in the diagram of figure 2B correspond to the foci of the ellipsoid to which the M_3 belongs. P coincides with the pivot point of M_2 while Q is located on the sample plane. The chief ray from the condenser mirror center C to the focus Q, forms an angle of 6° with the sample plane. By tilting M_2, it is possible to vary the chief ray angle of incidence on the sample surface without changing the position of the probe as shown in figure 2A.
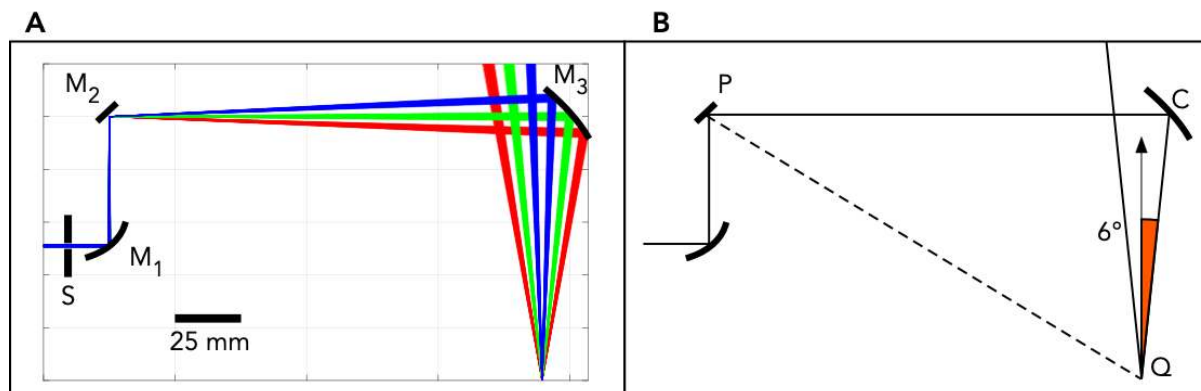

Figure 2. Optical layout of the Fourier synthesis illuminator. A. The EUV beam from the XIL-II beamline goes through a selectable aperture stop (S) and is reflected vertically and focused by the paraboloidal mirror M_1 in proximity of the surface of a tip-tilt mirror M_2. The beam is then focused on the sample by the ellipsoidal condenser mirror M_3. B. The two foci of the ellipsoid to which M_3 belongs are P, the pivot point of M_2, and Q, a point on the sample surface. The ray from the center C of M_3 to Q forms an angle of 6° with the normal to the sample plane.

The three mirrors that constitute the illuminator must be coated with a multilayer to ensure maximum reflection for EUV in the range of incidence angle they operate at. We calculated the angle of incidence distribution over the active surface of each of them and we verified that a suitable multilayer can be fabricated.

2.1 Paraboloidal mirror M$_1$

The XIL-II beamline produces a monochromatic EUV beam with a low divergence. With an aperture stop of 1 mm diameter, the beam divergence is 83×47 μrad^2. M_1 is an off-axis paraboloidal mirror that reflects the light from the beamline at 90º towards M_2 and focuses it 5 mm after the tip-tilt mirror surface. The aperture stop size and the focal length of M_1 determine the size of the beam footprint on M_2 and, as a consequence, the size of the probe on the sample. It is important to avoid to focus the beam on the surface of M_2 to limit the contamination, but at the same time, the beam footprint on M_2 can't be too large if we want to limit the size of the probe on the sample. The current design of the Fourier synthesis illuminator includes a single M_1 mirror with a focal length of 25 mm, an off-axis distance of $\overline{CF} = 50$ mm and a diameter of 25 mm (figure 3A). The beam footprint on the mirror and its angle of incidence distribution is shown in figure 3B. Given the relatively simple shape of the mirror and its small size, it is possible to equip the new system with multiple instances of M_1 with different focal lengths to allow a more flexible control of the illumination properties.
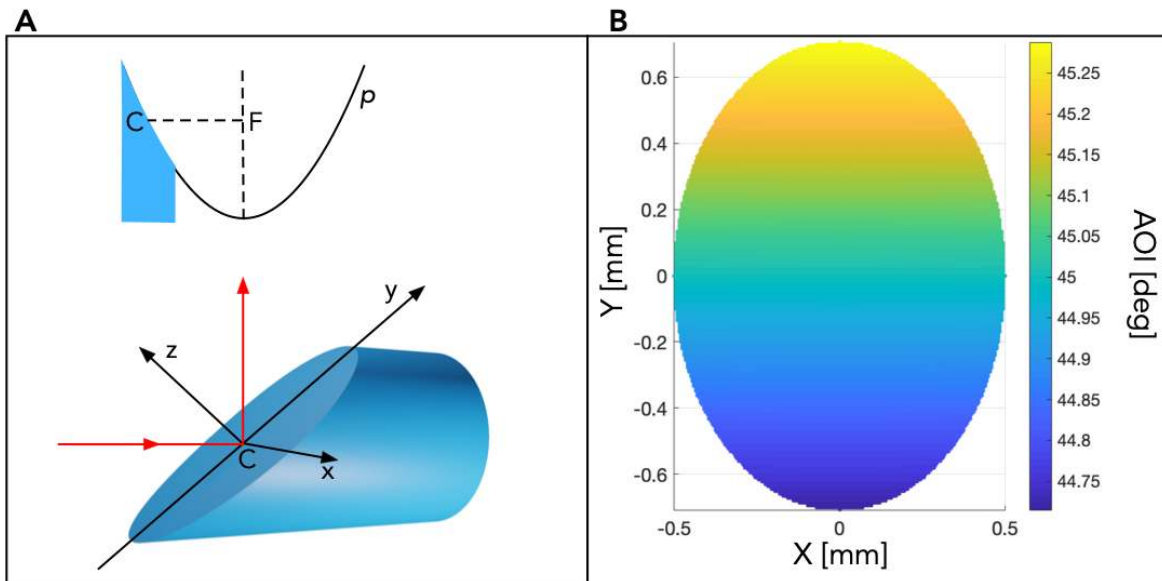

Figure 3. Angle of incidence on the surface of the M_1 mirror. A. Diagram of the geometry of M_1. The the z axis of the reference frame used to describe the properties of the surface of the mirror coincides with the normal to the surface at its center. The chief ray is shown in red. B. Footprint of the beam on the surface of the mirror and angle of incidence distribution.

2.2 Tip-tilt mirror M$_2$

The main concept of the Fourier synthesis illuminator is to control the angle of a pencil beam entering the illumination pupil. This functionality is provided by M_2, a flat tip-tilt mirror that reflects the beam focused by M_1 towards the condenser. M_2 will be mounted on a vacuum-compatible tip-tilt stage with a pivot point P coinciding with the mirror surface. This condition will ensure that the probe, which is the image of the beam footprint on a plane containing P and forming an angle of 6º with the chief ray (figure 2B), will remain stationary on the sample surface.

In its central configuration, M_2 forms an angle of 45º with the incoming chief ray and it can rotate around a fixed pivot point P located on its surface. The tip-tilt stage of the mirror has an angle range of ± 4º around the y axis and ± 3º around the x axis to cover the whole pupil defined by the condenser mirror M_3. This requirement implies that the the angle of incidence of the beam on M_2, showed in figure 4B for the central configuration, will actually go from 40º to 48º, requiring an optimized broad-band multilayer coating.

The estimated EUV flux on the surface of M_2 is 10^{11} photons/s. To prevent carbon deposition on the mirror surface, the system will operate in ultra-high vacuum, or in a controlled H_2 atmosphere, but, as an additional

measure, the mirror is designed with a rectangular shape in order to translate it laterally once the previously used area has become damaged or contaminated.
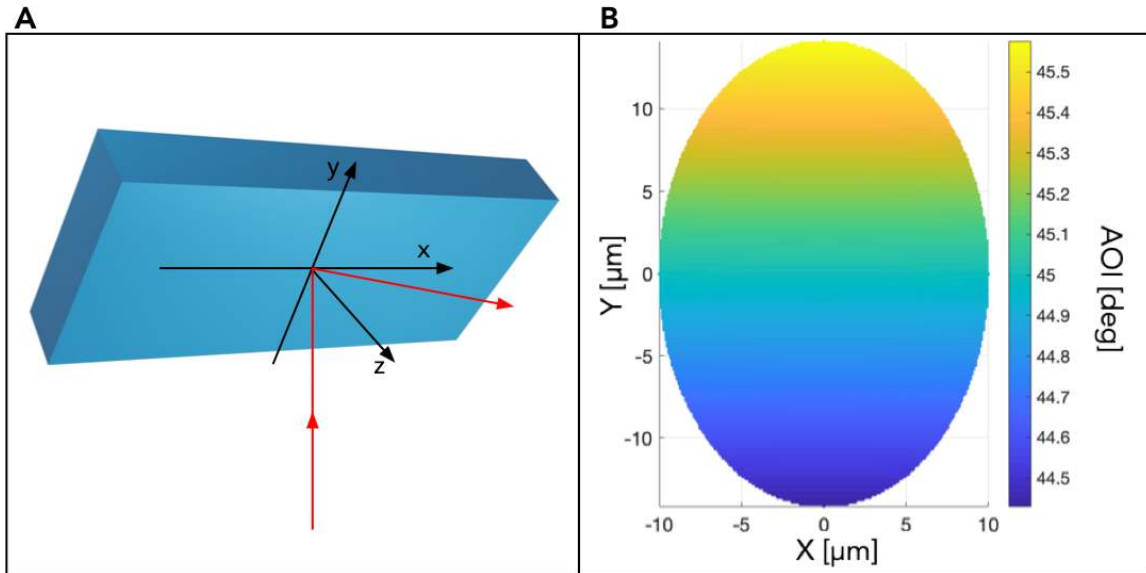

Figure 4. Angle of incidence on the surface of the M_2 mirror. A. Diagram of the geometry of M_2. The the z axis of the reference frame used to describe the properties of the surface of the mirror coincides with the normal to the surface at its center. The chief ray is shown in red. B. Footprint of the beam on the surface of the mirror and angle of incidence distribution when M_2 is in its central configuration.

2.3 Condenser mirror M₃

The beam steered by M_2 is reflected by M_3, an ellipsoidal condenser mirror with one focus located on P, the pivot point of the tip-tilt mirror, and the other on a point Q on the sample surface as shown in figure 2B. The center C of the condenser mirror is designed to reflect the chief ray so that $\vec{CQ}$ forms an angle of 6° with the normal to the sample surface. The active area of the mirror, shown in figure 5B, has a keystone shape with a maximum extension of 27 mm in y and 35 mm in x. The critical edge of this shape is the shorter arc at the bottom of the figure where the reflecting area must extend as much as possible towards the physical edge of the mirror to limit the vignetting of the light diffracted by the sample. A maximum edge of 1 mm can be tolerated. The footprint of the beam on M_3 is roughly elliptical with an extension of about 4 mm (figure 6A). The flux density on M_3 can be estimated as $6 \cdot 10^{10}$ photons/(s·mm²). The magnification of M_3 changes slightly with the illumination angle and the diameter of the probe on the sample varies from 9 to 11 μm for an aperture stop of 1 mm as shown in figure 6B. This is a not a problem for the image reconstruction algorithm employed in RESCAN because each illumination probe and its corresponding sample image is reconstructed independently.[4]

2.4 Multilayer specifications

The three mirrors of the illumination system work with different angles of incidence and they will need different multilayer designs to maximize their EUV reflectance. M_2 requires the largest range of incidence angles and for this reason, the design of its multilayer is the most critical. We verified the possibility to manufacture a suitable multilayer starting from a standard periodic Mo/Si stack. The required angle range to optimize is 40° to 48°, so we started with a periodic multilayer design with 40 Mo/Si bilayers and maximum reflectance centered at 44°. We optimized the thickness of each layer in order to minimize the merit function:

$$f(\vec{t}) = \int_{40°}^{48°} \left(R(\alpha, \vec{t}) - T(\alpha)\right)^2 d\alpha, \tag{4}$$
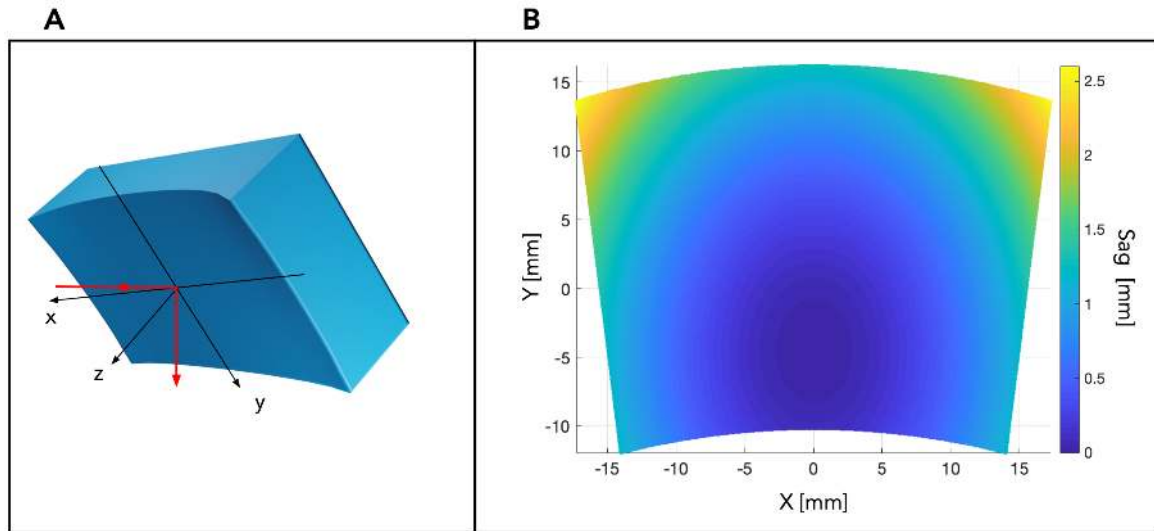
Figure 5. A. Diagram of the geometry of M_3. The z axis of the reference frame used to describe the properties of the surface of the mirror coincides with the normal to the surface at its center. The chief ray is shown in red. B. Sag plot of the active area of the reflective surface of M_3.
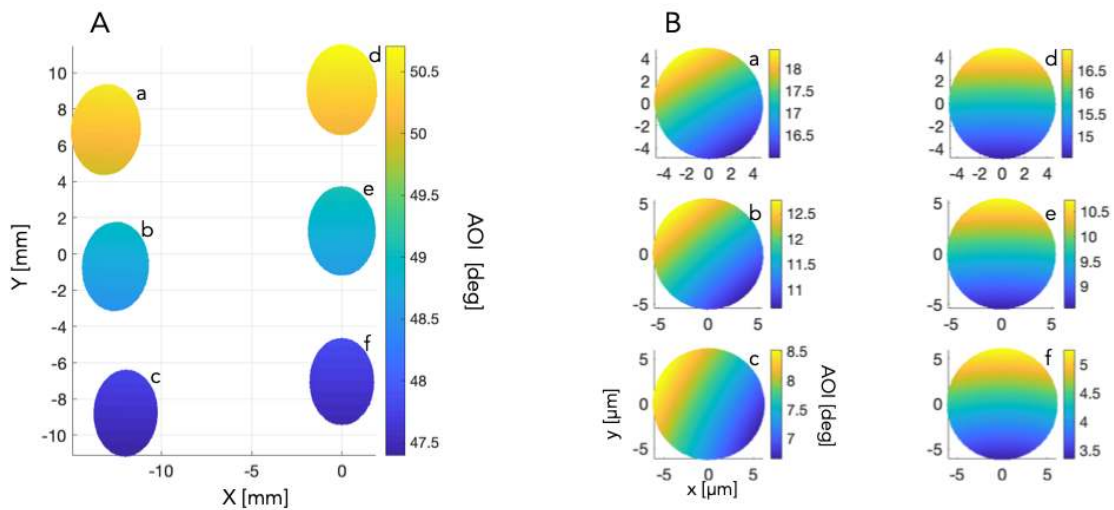

Figure 6. A. Position and angle of incidence of the beam on M_3 for six different angles of the tip tilt mirror. The reference frame used here is the same shown in figure 5A. B. Probe position and angle of incidence distribution on the sample surface.
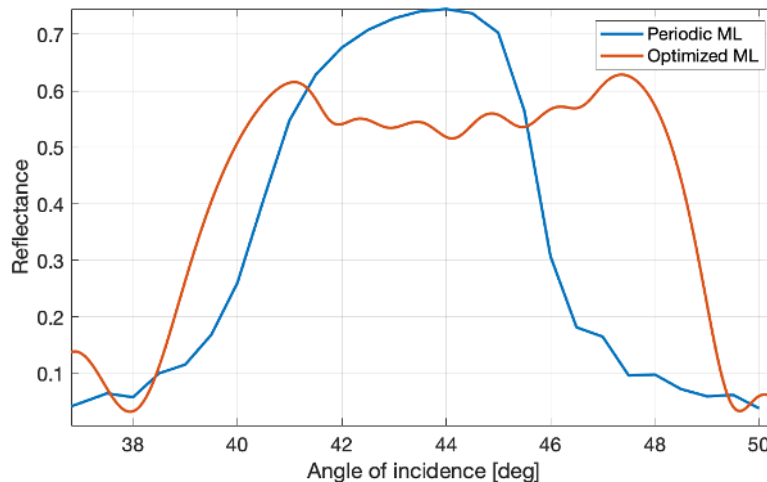
Figure 7. The blue curve represents the reflectance of a standard periodic Mo/Si multilayer with 40 bi-layers optimized for 13.5 nm and an angle of incidence of 44º. The red curve represents the reflectance of an a-periodic stack with the same number of layers optimized to cover a reflection angle range going from 40ºto 48º.

where $\vec{t}$ is a vector containing the thickness of each of the 80 layers, $R(\alpha, \vec{t})$ is the reflectance of the multilayer and $T(\alpha)$ is the target reflectance function.[9] To calculate the multilayer reflectance, we developed a customizable MATLAB® function[10] implementing a standard matrix multiplication method.[11] Figure 7 shows that, optimizing the thicknesses of the 40 bilayers, we can obtain a large bandwidth multilayer with a reflectance above 0.5. This result could be further improved using more layers as shown in previous research.[9,12]

3. OUTLOOK AND CONCLUSION

We designed a new optical system to provide the RESCAN lensless microscope with flexible coherence control capability and to overcome the fundamental resolution limitations caused by the characteristics of the EUV mask multilayer. The system consists of a Fourier synthesis illuminator that will allow to change the illumination angle without displacing the probe on the sample. The illuminator has been developed with the goal to optimize several parameters of the microscope while keeping a flexible and affordable design to enable future upgrades when needed. The new illuminator, which will be implemented in the current RESCAN microscope, will be also a test bed for the potential development of a new lensless microscope for EUV mask metrology. This new microscope will be the evolution of the current RESCAN platform which was developed to demonstrate the potential of coherent diffraction imaging for EUV mask inspection. The concept is summarized in figure 8 and will include an x, y reticle stage with interferometric position feedback, an optical microscope for pattern registration and navigation, and an automated mask loading system to avoid sample contamination. It will also feature an upgraded version of the Fourier synthesis illumination system described in this paper that will make it suitable for both mask inspection and review. With a maximum synthetic numerical aperture of 0.24 the system will have an imaging resolution of 28 nm on mask or 7 nm on wafer and will be able to provide reliable actinic mask metrology for the current and future technology nodes.
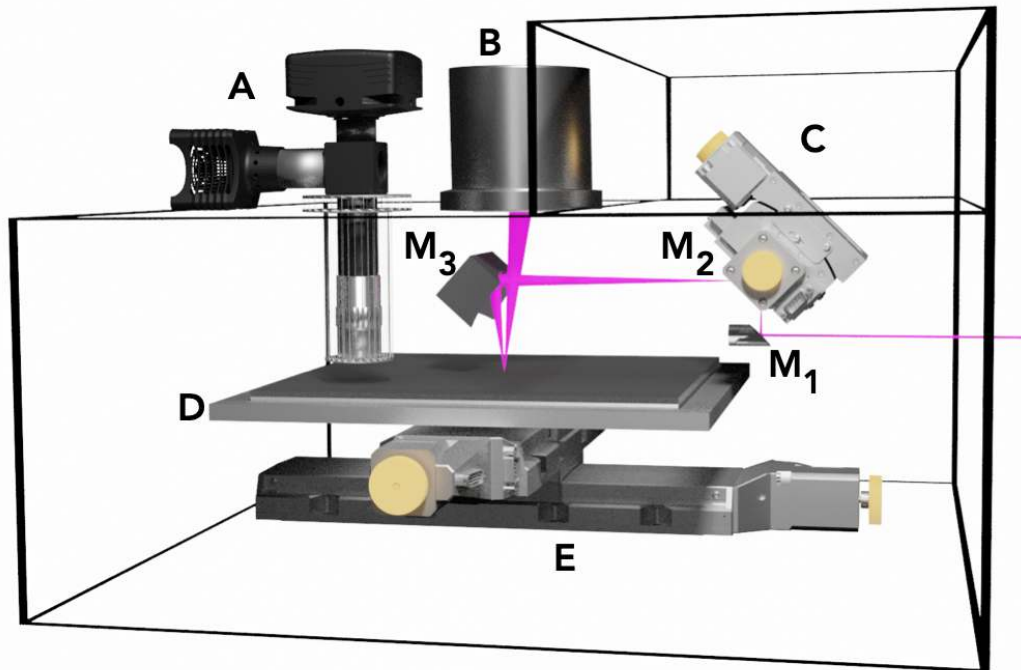
ACKNOWLEDGMENTS

Figure 8. Conceptual rendering of a new, synchrotron-based lensless microscope for EUV mask inspection and review. A is a visible-light microscope for sample navigation, B is an EUV pixel detector, C is the tip-tilt stage for the M_2 mirror, D is the reticle holder, E is an x, y stage with interferometric position feedback.

REFERENCES

[1] Capelli, R., Dietzel, M., Hellweg, D., Koch, M., Kersteen, G., Gwosch, K., and Pagel, D., "Actinic metrology platform for defect review and mask qualification: flexibility and performance," *Proc.SPIE* **10957** (2019). doi:10.1117/12.2518596.

[2] Miyai, H., Kohyama, T., Suzuki, T., Takehisa, K., and Kusunose, H., "Actinic patterned mask defect inspection for EUV lithography," in [*Photomask Technology 2019*], Rankin, J. H. and Preil, M. E., eds., *Proc.SPIE* **11148**, 162 – 170 (2019). doi:10.1117/12.2538001.

[3] Mochi, I., Fernandez, S., Nebling, R., Locans, U., Helfenstein, P., Rajeev, R., Dejkameh, A., Kazazis, D., Tseng, L.-T., and Ekinci, Y., "Absorber and phase defect inspection on euv reticles using RESCAN," *Proc.SPIE* **10957** (2019). doi:10.1117/12.2515160.

[4] Mochi, I., Locans, U., Dejkameh, A., Nebling, R., Kazazis, D., Tseng, L.-T., and Ekinci, Y., "Resolution enhancement for lensless mask metrology with RESCAN," *Proc.SPIE* **11147**, 156 – 163 (2019). doi:10.1117/12.2537068.

[5] Naulleau, P. P., Goldberg, K. A., Batson, P., Bokor, J., Denham, P., and Rekawa, S., "Fourier-synthesis custom-coherence illuminator for extreme ultraviolet microfield lithography," *Appl. Opt.* **42**, 820–826 (Feb 2003).

[6] Mochi, I., Goldberg, K. A., Benk, M. P., and Naulleau, P. P., "Pupil shaping and coherence control in an EUV mask-imaging microscope," in [*Photomask Technology 2013*], Faure, T. B. and Ackmann, P. W., eds., *Proc.SPIE* **8880**, 315 – 324 (2013).

[7] van der Veen, F. and Pfeiffer, F., "Coherent x-ray scattering," *Journal of Physics: Condensed Matter* **16**, 5003–5030 (jul 2004).

[8] Williams, G. J., Quiney, H. M., Peele, A. G., and Nugent, K. A., "Fresnel coherent diffractive imaging: treatment and analysis of data," *New Journal of Physics* **12**, 035020 (mar 2010).

[9] Kuhlmann, T., Yulin, S. A., Feigl, T., and Kaiser, N., "EUV multilayer mirrors with tailored spectral reflectivity," in [*X-Ray Mirrors, Crystals, and Multilayers II*], Freund, A. K., Macrander, A. T., Ishikawa, T., and Wood, J. L., eds., *Proc.SPIE* **4782**, 196 – 203 (2002). doi:10.1117/12.451348.

[10] Mochi, I., "Multilayer-mirror." https://zenodo.org/badge/latestdoi/207020995 (September 2019).

[11] Hecht, E., [*Optics (4th Edition)*], 426–428, Addison-Wesley (2001).

[12] Wang, Z., "Non-periodic multilayer coatings in EUV, soft x-ray and x-ray range," in [*Advances in Optical Thin Films III*], Kaiser, N., Lequime, M., and Macleod, H. A., eds., *Proc.SPIE* **7101**, 373 – 387 (2008). doi:10.1117/12.797156.